ELSEVIER

Journal of Alloys and Compounds 444–445 (2007) 154–161

Journal of ALLOYS AND COMPOUNDS

www.elsevier.com/locate/jallcom

Beyond spin-orbit: Probing electron correlation in the Pu 5f states using spin-resolved photoelectron spectroscopy

J.G. Tobin *

Lawrence Livermore National Laboratory, Livermore, CMS 7000 East Ave, L-356, Livermore, CA 94550, USA

Received 11 May 2006; received in revised form 17 October 2006; accepted 23 October 2006
Available online 14 December 2006

Abstract

Experiments planned to address the issue of electron correlation in the Pu 5f states are described herein. The key is the utilization of the Fano effect: the observation of spin polarization in nonmagnetic systems, using chiral excitation such as circularly polarized X-rays.

Keywords: Metals; Electronic states (localized); Electronic band structure; Photoelectron spectroscopies; Synchrotron radiation; NEXAFS

1. Introduction

The enigma of Plutonium (Pu) electronic structure is being unraveled. Sixty years after its discovery, the mystery of the electronic structure of Pu is finally being resolved. In a series of experiments and linked theoretical modeling, the range of possible solutions for Pu electronic structure has been dramatically reduced.

The approach is to experimentally determine which potential terms are the largest.

$$H\Psi = -(\nabla^2/2m)\Psi + V\Psi,$$
$$\text{where } V = V_1 + V_2 + V_3 + V_4 + \ldots$$

Synchrotron-radiation-based X-ray absorption, electron energy-loss spectroscopy in a transmission electron microscope, multi-electronic atomic spectral simulations and first principles calculations (generalized gradient approximation in the local density approximation (GGA/LDA)) have been used to investigate the electronic structure of plutonium [1–4]. From these studies, the following key insights have been gleaned.

1. Russell–Saunders coupling fails for Pu. Pu is a jj-skewed intermediate coupling case, with a large 5f spin-orbit coupling.
2. The number of 5f electrons in Pu is approximately five.
3. Spin orbit splitting dominates delocalization effects: $V_{SO} > V_{Delocalization}$, to the point that the Pu 5f states can be viewed as predominantly localized.

The remaining issues for Pu electronic structure are primarily those of electron correlation effects. Based upon the success of magnetic methods in explaining the physical properties of the different phases of Pu [5–10], it is possible to hypothesize that for δ-Pu there are strong indications that V_{MAG} perturbs V_{SO} and $V_{MAG} > V_{Delocalization}$. In Pu, it is expected to observe large but counter aligned spin and orbital polarizations or magnetic moments within the 5f manifold. The counter alignment should lead to substantial cancellation. However, there would be need to an additional shielding or cancellation going on in δ-Pu, such as Kondo shielding [11–13], spin fluctuation [14], non-collinearity [15], or averaging [10]. In any case, the magnetic cancellation must be complete: Pu has no net magnetic moment [16,17]. Alternatively, there is the possibility that there are no magnetic substructures and that the electron correlation is a type of pure Kondo shielding best described by dynamical mean field theory [11–13]. These last two issues can be resolved with the Fano effect measurements, as will be described below.

The approach is founded upon a model in which magnetic and spin-orbit splittings are included in the picture of the 5f states and upon the observation of chiral/spin-dependent effects in non-magnetic systems. By extending a quantitative model developed for the interpretation of core level spectroscopy in magnetic systems, it is possible to predict the contributions of

* Tel.: +1 925 422 7247; fax: +1 925 423 7040.

0925-8388/$ – see front matter © 2006 Elsevier B.V. All rights reserved.
doi:10.1016/j.jallcom.2006.10.107

the individual component states within the 5f manifold. This has lead to a remarkable agreement between the results of the model and the previously collected spectra of δ-Pu(Ga).

2. Estimating the magnitude of the magnetic substructure with XAS

It is important to digress for a moment and reconsider the Pu density of states (DOS). In a recent PRB [4], Kutepov calculated both non-magnetic (NM) and anti-ferromagnetic (AF) DOS (Fig. 1). Both agree qualitatively with the simple picture derived from spectroscopic results. The NM and AF limits are related, being on opposite ends of the plot below in Fig. 1. (For NM, $H_s/\zeta = 0$, and for AF, the extreme limit would be $Hs/\zeta > 10$. Here H_s = spin field (exchange) and ζ = spin-orbit parameter). The spectrum labeled AF is, in fact, an intermediate solution, where the spin-orbit splitting and exchange splitting are of the same order of magnitude. Is it possible to derive the characteristics of the intermediate solution directly from experimental data?

One way to extract the possible size of the magnetic perturbation would be to analyze the X-ray absorption branching ratio of Pu for the 4d to 5f excitation, assuming a jj limit with a magnetic splitting. This has been done and the result is shown below in Tables 1 and 2 and Figs. 2–5. (It should be noted that the EELS results for α-Pu and δ-Pu are essentially identical with each other and with the XAS result for α-Pu [3]).

Table 1
Orthogonalized initial 5f states

$[1> = [3, 1/2>$
$[2> = \cos\theta_2\ [2, 1/2> + \sin\theta_2\ [3, -1/2>$
$[3> = \cos\theta_3\ [1, 1/2> + \sin\theta_3\ [2, -1/2>$
$[4> = \cos\theta_4\ [0, 1/2> + \sin\theta_4\ [1, -1/2>$
$[5> = \cos\theta_5\ [-1, 1/2> + \sin\theta_5\ [0, -1/2>$
$[6> = \cos\theta_6\ [-2, 1/2> + \sin\theta_6\ [-1, 1/2>$
$[7> = \cos\theta_7\ [-3, 1/2> + \sin\theta_7\ [-2, -1/2>$
$[8> = [-3, -1/2>$
$[9> = -\sin\theta_7\ [-3, 1/2> + \cos\theta_7\ [-2, -1/2>$
$[10> = -\sin\theta_6\ [-2, 1/2> + \cos\theta_6\ [-1, -1/2>$
$[11> = -\sin\theta_5\ [-1, 1/2> + \cos\theta_5\ [0, -1/2>$
$[12> = -\sin\theta_4\ [0, 1/2> + \cos\theta_4\ [1, -1/2>$
$[13> = -\sin\theta_3\ [1, 1/2> + \cos\theta_3\ [2, -1/2>$
$[14> = -\sin\theta_2\ [2, 1/2> + \cos\theta_2\ [3, -1/2>$
$2\theta_2 = \arctan\,(2.4995/(2.5 + H_s/\zeta)) \geq 0$
$2\theta_3 = \arctan\,(3.1623/(1.5 + H_s/\zeta)) \geq 0$
$2\theta_4 = \arctan\,(3.4641/(0.5 + H_s/\zeta)) \geq 0$
$2\theta_5 = \arctan\,(3.4641/(-0.5 + H_s/\zeta)) \geq 0$
$2\theta_6 = \arctan\,(3.1623/(-1.5 + H_s/\zeta)) \geq 0$
$2\theta_7 = \arctan\,(2.4995/(-2.5 + H_s/\zeta)) \geq 0$

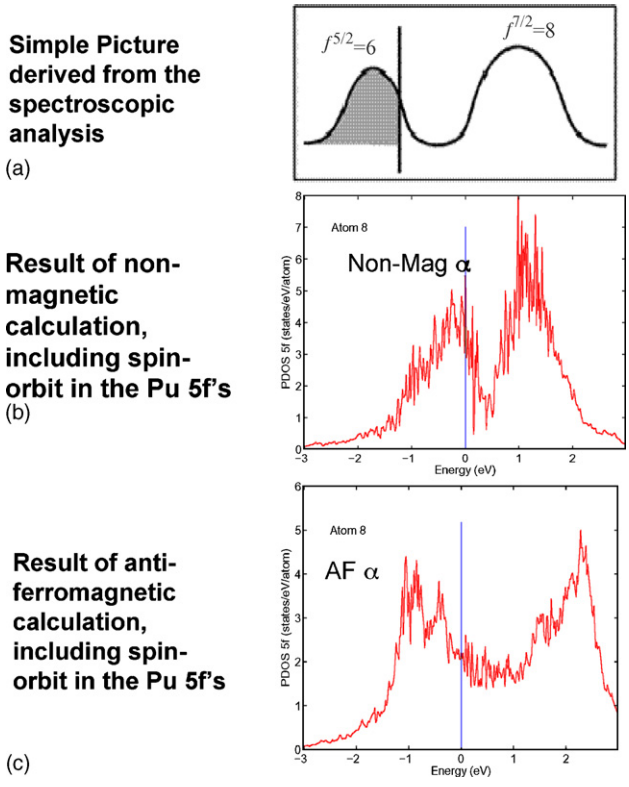

Fig. 1. (a) Simple picture derived from the spectroscopic analysis. (b) Result of non-magnetic calculation, including spin-orbit in the Pu 5F's. (c) Result of anti-ferromagnetic calculation, including spin-orbit in the Pu 5F's.

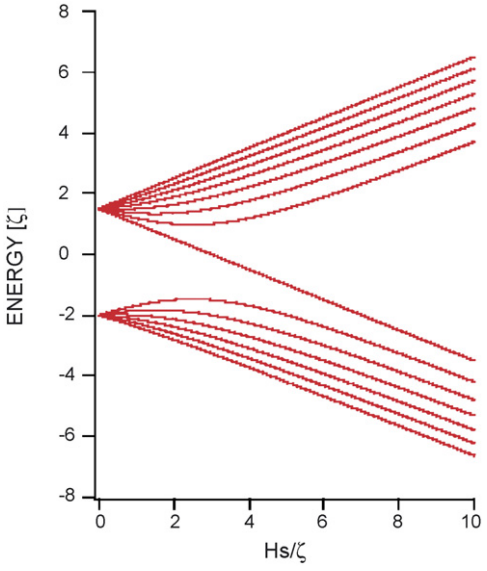

Fig. 2. Here is a picture of the energy of the orthogonalized states as a function of the ratio of the exchange and spin orbit splittings. H_s is the "spin field" or exchange splitting between states 1 and 8. (The states are numbered 1–14, starting at the top). ζ is the spin-orbit splitting parameter. For Th through Am, only the lower states, 14 through 9, will be occupied.

Table 2
Energies of the orthogonalized 5f states

$E_1 = H_s/\zeta*0.5 + 1.5$
$E_2 = H_s/\zeta*(-0.5 + (\cos\theta_2)^2) + 1.0*(\cos\theta_2)^2 - 1.5*(\sin\theta_2)^2 + (\cos\theta_2)*(\sin\theta_2)*2.4495$
$E_3 = H_s/\zeta*(-0.5 + (\cos\theta_3)^2) + 0.5*(\cos\theta_3)^2 - 1.0*(\sin\theta_3)^2 + (\cos\theta_3)*(\sin\theta_3)*3.1623$
$E_4 = H_s/\zeta*(-0.5 + (\cos\theta_4)^2) + 0*(\cos\theta_4)^2 - 0.5*(\sin\theta_4)^2 + (\cos\theta_4)*(\sin\theta_4)*3.4641$
$E_5 = H_s/\zeta*(-0.5 + (\cos\theta_5)^2) - 0.5*(\cos\theta_5)^2 - 0*(\sin\theta_5)^2 + (\cos\theta_5)*(\sin\theta_5)*3.4641$
$E_6 = H_s/\zeta*(-0.5 + (\cos\theta_6)^2) - 1.0*(\cos\theta_6)^2 + 0.5*(\sin\theta_6)^2 + (\cos\theta_6)*(\sin\theta_6)*3.1623$
$E_7 = H_s/\zeta*(-0.5 + (\cos\theta_7)^2) - 1.5*(\cos\theta_7)^2 + 1.0*(\sin\theta_7)^2 + (\cos\theta_7)*(\sin\theta_7)*2.4495$
$E_8 = -H_s/\zeta*0.5 + 1.5$
$E_9 = -H_s/\zeta*(-0.5 + (\cos\theta_7)^2) - 1.5*(\sin\theta_7)^2 + 1.0*(\cos\theta_7)^2 - (\cos\theta_7)*(\sin\theta_7)*2.4495$
$E_{10} = -H_s/\zeta*(-0.5 + (\cos\theta_6)^2) - 1.0*(\sin\theta_6)^2 + 0.5*(\cos\theta_6)^2 - (\cos\theta_6)*(\sin\theta_6)*3.1623$
$E_{11} = -H_s/\zeta*(-0.5 + (\cos\theta_5)^2) - 0.5*(\sin\theta_5)^2 - 0*(\cos\theta_5)^2 - (\cos\theta_5)*(\sin\theta_5)*3.4641$
$E_{12} = -H_s/\zeta*(-0.5 + (\cos\theta_4)^2) + 0*(\sin\theta_4)^2 - 0.5*(\cos\theta_4)^2 - (\cos\theta_4)*(\sin\theta_4)*3.4641$
$E_{13} = -H_s/\zeta*(-0.5 + (\cos\theta_3)^2) + 0.5*(\sin\theta_3)^2 - 1.0*(\cos\theta_3)^2 - (\cos\theta_3)*(\sin\theta_3)*3.1623$
$E_{14} = -H_s/\zeta*(-0.5 + (\cos\theta_2)^2) + 1.0*(\sin\theta_2)^2 - 1.5*(\cos\theta_2)^2 - (\mathrm{co\,s}\theta_2)*(\sin\theta_2)*2.4495$
$2\theta_2 = \arctan(2.4995/(2.5 + H_s/\zeta)) \geq 0$
$2\theta_3 = \arctan(3.1623/(1.5 + H_s/\zeta)) \geq 0$
$2\theta_4 = \arctan(3.4641/(0.5 + H_s/\zeta)) \geq 0$
$2\theta_5 = \arctan(3.4641/(-0.5 + H_s/\zeta)) \geq 0$
$2\theta_6 = \arctan(3.1623/(-1.5 + H_s/\zeta)) \geq 0$
$2\theta_7 = \arctan(2.4995/(-2.5 + H_s/\zeta)) \geq 0$

There are several steps in this process. First, the orthogonalized initial states must be generated, following the procedure developed previously for shallow core levels in a magnetic system [18]. The resultant states and their energy dependence are shown in Tables 1 and 2 and Fig. 2. Next, the state-to-state matrix elements must be calculated for the cases of linearly polarized X-rays, consistent with the experiments performed at the Advanced Light Source [1–4]. To do that, it is necessary to calculate the circular-polarization-driven transition moments (Fig. 3) and then sum properly. From there, it is then possible to predict how the branching ratio, $B = A_{5/2}/(A_{5/2} + A_{3/2})$ with A as the intensity at each edge, will change as the magnetic effect is increased, as shown in Fig. 4.

Thus, the Pu 4d to 5f XAS data (inset in Fig. 4) has been analyzed with a simple one electron picture with five electrons in the 5f level ($n = 5$), magnetically polarized 5f states, and linear photon polarization, including the correct state to state transition cross sections within the electric dipole approximation. The branching ratio analysis gives the result that $H_s/\zeta = 2.5$ (see Fig. 4). From Kutepov's calculations it is known that $\Delta E_{SO} \approx 2$ eV and using $Hs/\zeta = 2.5$, $\Delta E_{MAG} \approx 0.2$ eV is obtained (see Fig. 5).

3. Comparison to PES experimental results

The new model can explain the "regular" photoemission results for δ-Pu (Fig. 6). Using the value of $Hs/\zeta = 2.5$ and including the correct state to state transition cross sections within the electric dipole approximation for photoelectron spectroscopy (PES), the magnetic perturbation model ($V_{SO} + V_{MAG}$) gives fairly good agreement with our data, bulk δ and bulk α with a δ reconstruction: at worst, the model result is semi-quantitatively correct. Interestingly, the model is closer to the results of Butterfield et al. [19], where the small remaining oxygen-driven contributions have been reduced even further. Please note that the model has no delocalization nor hybridization in it. In the 5f states, delocalization and hybridization are essentially the same. Thus, the result of this analysis suggests that hybridization and delocalization play a role in the δ-Pu 5f states but it is a TERTIARY role ... $V_{SO} > V_{MAG} > V_{Delocalization}$.

Before progressing further, it is useful to consider how the simulated photoelectron spectrum was obtained. Again, state-to-state calculations are performed for the case consistent with the experimental set up, i.e. linear polarization, following the procedure developed earlier [18]. Also again, it begins with the strong selection rules of the circular polarization cases and then summing appropriately. The initial states are the occupied 5f states with the energy dependences shown in Fig. 2. The possible intensity for each state will depend upon the value of H_s/ζ, as shown in Fig. 7. For δ-Pu, it is assumed that the occupancy is 5.1 [5]. Thus, states 14, 13, 12, 11, and 10 are fully occupied and state 9 is only partially occupied (0.1) and tied to the Fermi energy. Only occupied states will contribute to PES, each in proportion to its occupation. The final state is a plane wave at normal emission, directed into the electron analyzer. Both final states, d-wave and g-wave, were considered, as shown in Table 2. (It is also possible to obtain spin dependent dichroisms for each state, as well as a preliminary estimate of the magnetic moments, as shown in Fig. 7. The spin dichroisms will be discussed in more detail below). To obtain a spectrum, however, it is also necessary to have an estimate of (1) peak shape and (2) the energy placement of the states. Here, a Doniach–Sunjic lineshape (Fig. 8) has been used, for each specific occupied initial state. The parameters used followed the guidelines below.

1. The DS-asymmetry parameter was 0.3 throughout.
2. The intensity and dichroism values for each state, 9 through 14, were kept constant throughout. The values used corresponded to the case of $H_s/\zeta \ll 1$ and for the f to d transition.

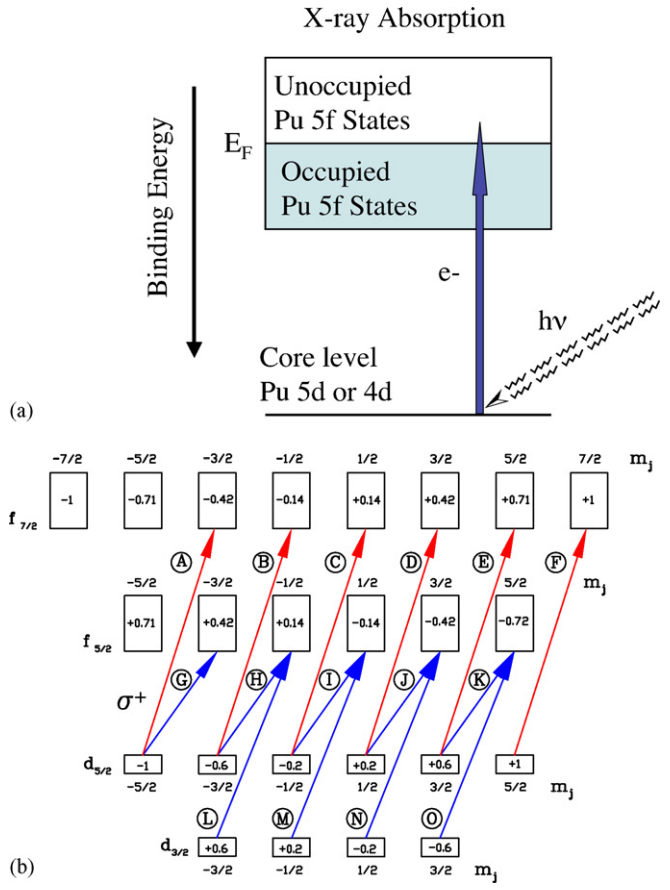

Fig. 3. (a) Schematic illustration of the X-ray absorption process. E_F is the Fermi level, the energy level between the occupied and unoccupied states. The photon ($h\nu$) is absorbed, moving the core level electron (e-) up into the unoccupied states. (b) Example of XAS electric dipole transitions for pure spin orbit split states. Scheme of the photoexcitation d to f with positive helicity. The arrows indicate the allowed transitions via relativistic dipole selection rules for positive helicity with the following transition probabilities normalized to transition G. A = 5/2, B = 15/2, C = 30/2, D = 50/2, E = 75/2, F = 105/2, G = 1, H = 8/5, I = 9/5, J = 8/5, K = 1, L = 49/10, M = 147/10, N = 147/5, O = 49. Thereby, identical radial parts of the $d_{5/2}$ and $d_{3/2}$ wave functions and of the $f_{7/2}$ and $f_{5/2}$ wave functions are assumed. The arrows with red (blue) color represent transitions, which give positive (negative) spin polarization of photoelectrons. Positive and negative numbers in the rectangles give the angle integrated spin polarization for given mj using Clebsch–Gordan coefficients. Energy differences are not to scale. For more detail, see [24]. Note that $d_{3/2}$ to $f_{7/2}$ transitions are forbidden for pure spin orbit split states. Courtesy of Sung Woo Yu.

Table 3
Here are shown the PES intensity magnitudes (M_L) for linearly polarized excitation and spin dichroisms (D_c) for circularly polarized excitation, for a final state of g wave and f wave character

m_{5f}	$M_L{}^g$	$D_c{}^g$	$M_L{}^d$	$D_c{}^d$
3	1	−1	1	1
2	0	0	0	0
1	0.318	−1/5	0.244	1/5
0	0	0	0	0
−1	0.318	1/5	0.244	−1/5
−2	0	0	0	0
−3	1	1	1	−1

Relative intensities between columns depend upon various radial matrix elements and are thus photon energy dependent. Each column normalized such that the largest value equals one.

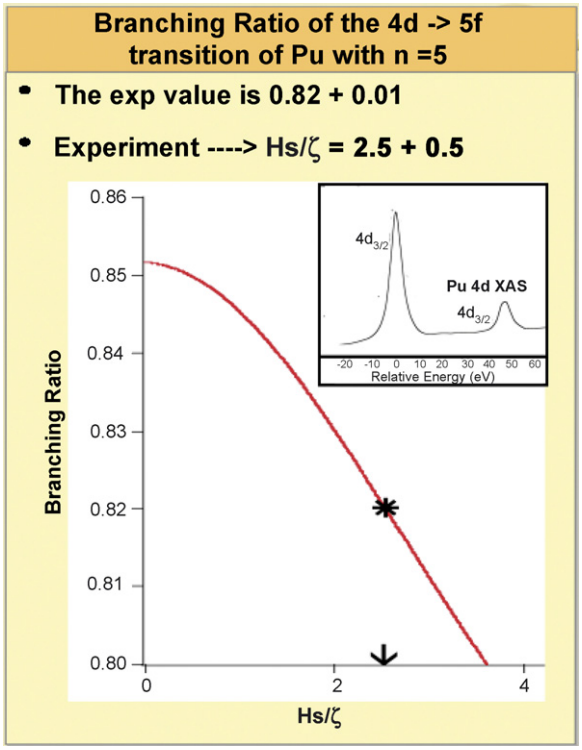

Fig. 4. Here is shown the experimental determination of the H_s/ζ ratio from the experimental XAS Pu branching ratio (B) and a simple model including the effect of both spin-orbit splitting and magnetic splitting.

By using the values corresponding to $H_s/\zeta \ll 1$, the effects of errors in the determination of H_s/ζ are minimized. As shown in Table 3, the matrix elements for the f to g-wave and f- to d-wave are very similar for the intensities and differ only by a negative sign in the dichroism.

3. The lifetime peak-width value was extracted from the experimental Am He-ll spectrum of Naegele [20]. The lifetime values were proportional to the Am value and allowed to

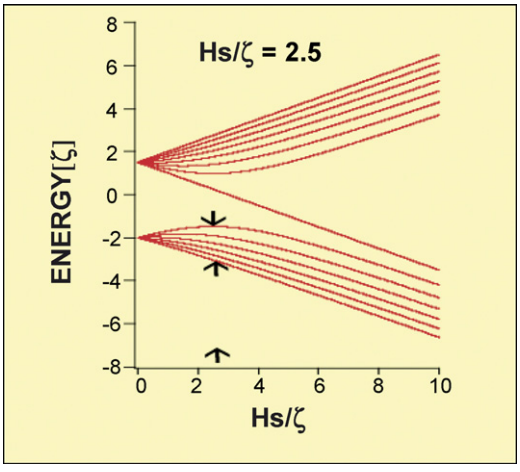

Fig. 5. Shown here are the energy values of the orthogonalized 5f component states (in units of ζ) as a function of the ratio of exchange (H_s) and spin orbit (ζ) splittings. At $H_s/\zeta = 2.5$, $\Delta E_{MAG} \approx 0.2$ eV, from $\zeta \approx 0.57$ eV, $\Delta E_{SO} \approx 2$ eV and $\Delta E_{SO} = 7\zeta/2$.

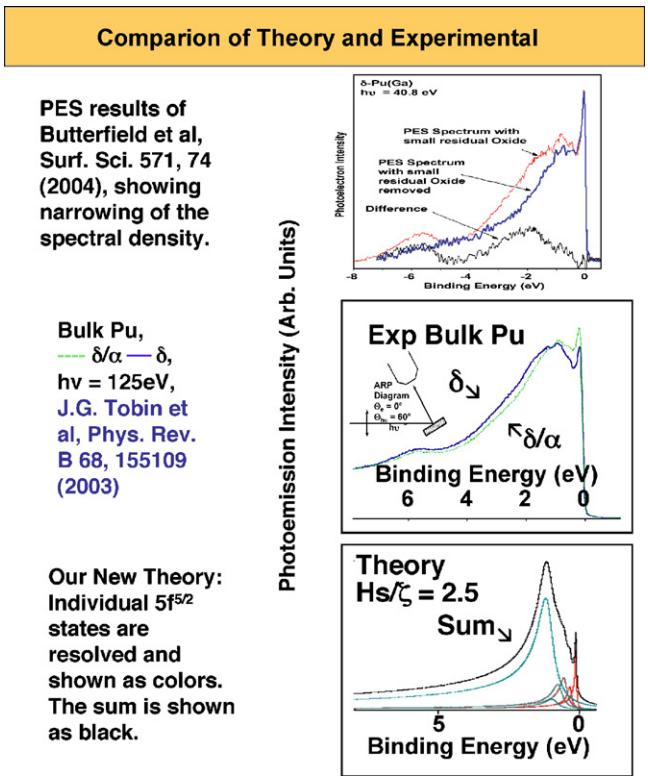

Fig. 6. Photoelectron spectroscopy (PES) experiment and theory are shown here. The theory here is not density of states (DOS) but rather spectral simulations with correct state-to-state matrix elements.

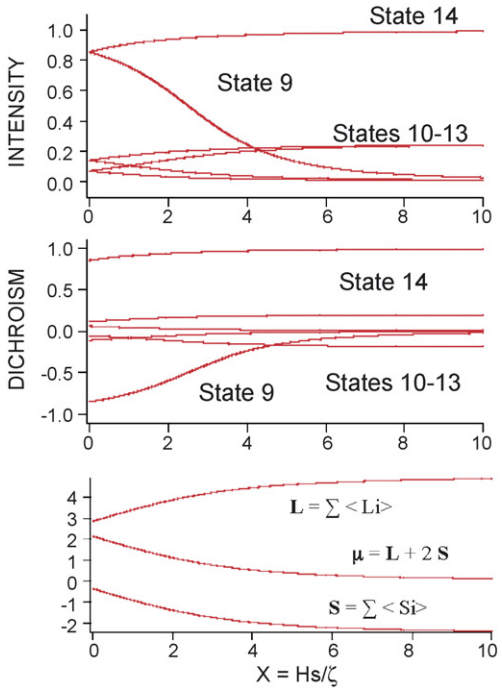

Fig. 7. Shown here are predictions of strong intensities and reversed dichroisms from states 9 and 14, for f to d-wave transitions. Similar results occur for the f to g transitions (not shown). H_s/ζ is the exchange/spin orbit splitting ratio. From the model, one can calculate the 5f spin, 5f orbital and 5f total moments vs. H_s/ζ, assuming the Pu 5f electrons are metallic and do not experience angular momentum coupling, i.e., following Savrosov and Kotliar [5]. These magnetic moments are the projections along the z axis.

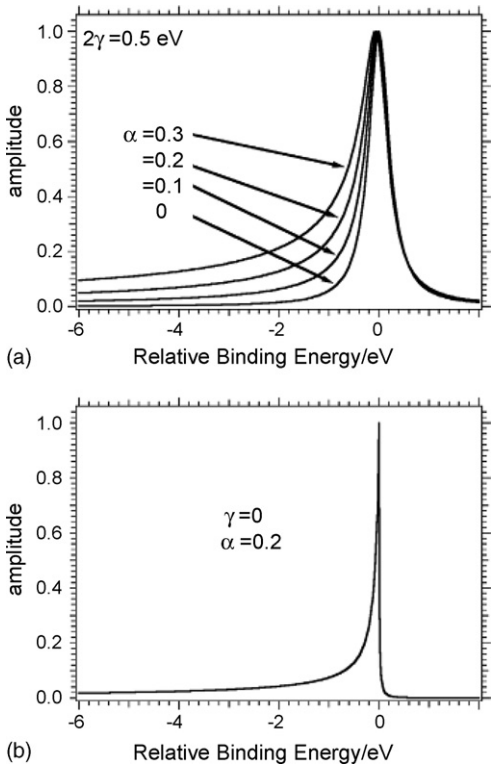

Fig. 8. Shown here are the (a) DS line-shapes and (b) the DS asymmetry.

diminish linearly to zero as binding energy went to zero, for each individual state.

4. The tentative "exchange splitting" value was extracted from our experimental Pu XAS spectrum, as described above, with an effective value of approximately 0.2 eV.
5. No further optimization of parameters was performed.

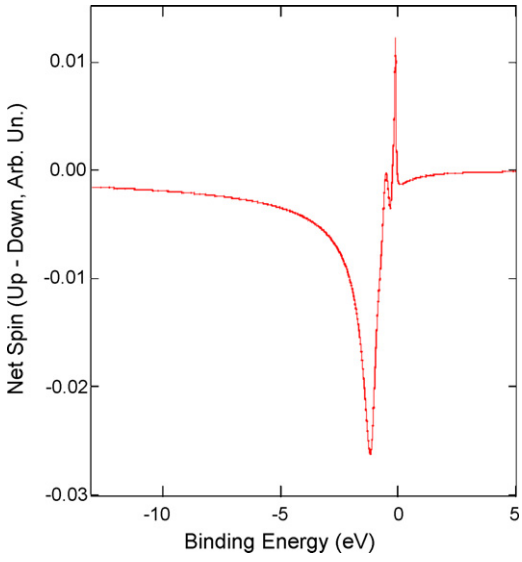

Fig. 9. Above is our prediction of the dichroism in δ-Pu. Double polarization photoelectron dichroism is the ideal technique with which to probe for such a dynamically shielded moment, with (1) a probe time on the scale of 10^{-15} s and (2) the capability to see spin effects in non-magnetic materials.

4. Spin polarized PES measurements

The acid test of the new model of Pu electronic structure will be the spin dependence. Using the Fano effect (double polarization photoelectron dichroism), strong spin dependence in non-magnetic Pu should be observed, as shown in Fig. 9. The Fano Effect is the emission of spin polarized electrons by non-magnetic materials, when excited by circularly polarized photons, as predicted by U. Fano [21] and measured shortly thereafter [22–24]. Fano dichroism PES is the ideal technique with which to probe for such a dynamically shielded moment, with (1) a probe time on the scale of 10^{-15} s and (2) the capability to see spin effects in non-magnetic materials.

At this point, it is useful to digress again and consider the "Fano effect" and its special characteristics in more detail. It is believed that Fano effect measurements (aka double polarization

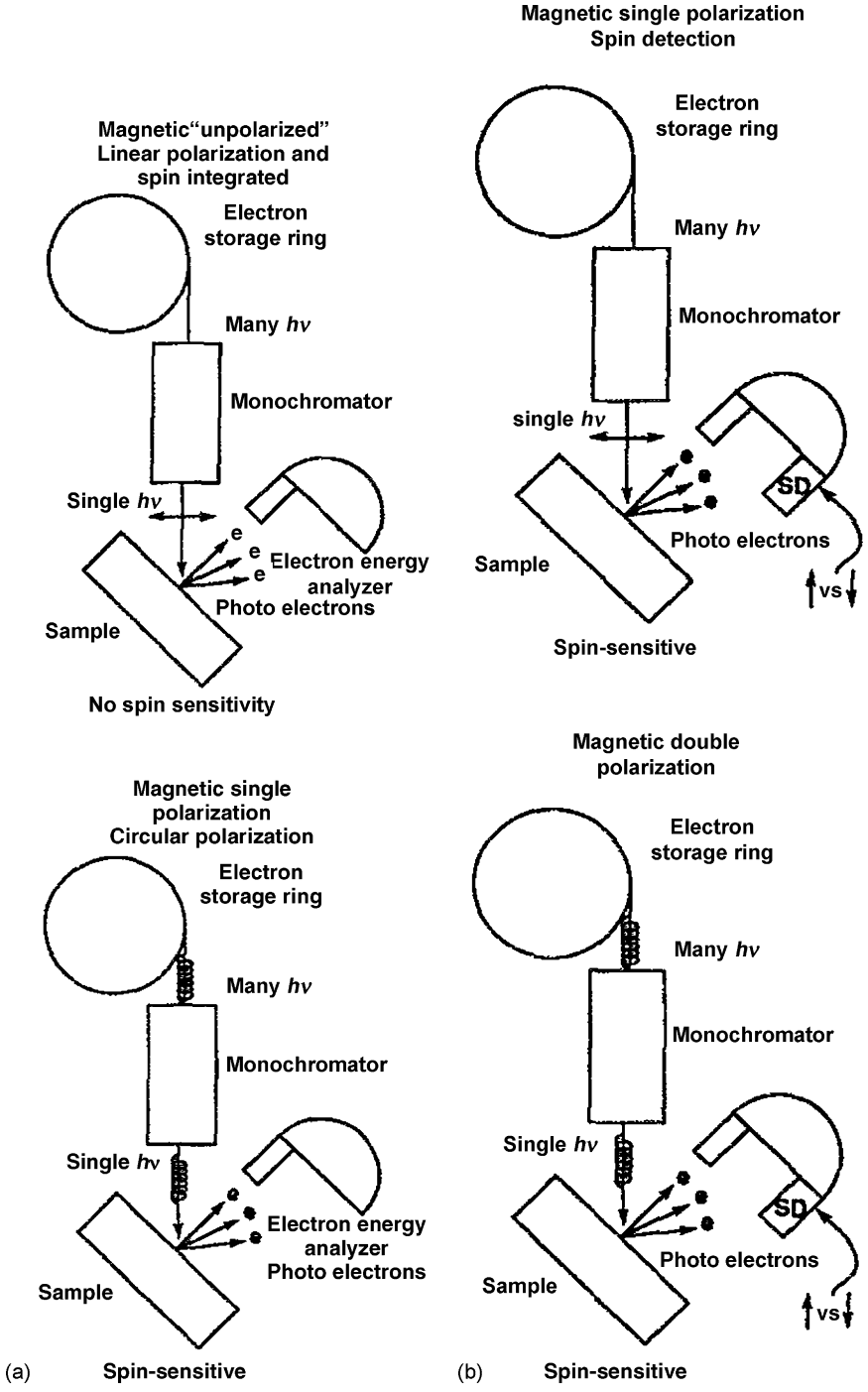

Fig. 10. Top left: unpolarized; bottom left: single polarization due to circularly polarized X-rays; top right: single polarization due to spin detection; bottom right: double polarization photoelectron dichroism. It should be noted that although the "unpolarized" case with linear polarization is shown, it is possible to use linearly polarized or unpolarized X-radiation as part of a chiral arrangement, to achieve X-ray magnetic linear dichroism in PES. Here the chiral arrangement of vectors essentially mimics the intrinsic chirality of the circularly polarized X-rays.

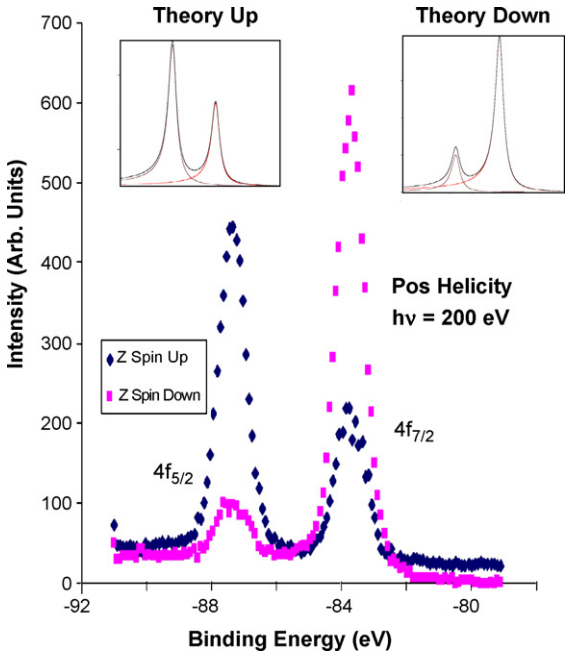

Fig. 11. Shown here are the experimental results for the Au 4f states, without background subtraction, as well as the results of the model.

photoelectron spectroscopy (DPPS)) are the key to unraveling the electron correlation in Pu. In Fano effect measurements, one uses a chiral excitation and true spin detection of the electrons in non-magnetic materials to gain detailed information about the valence band electronic structure of these materials. In ferro-magnetic systems, it is only necessary to have only single polarization because of the presence of the macroscopic magnetization vector. In the case of ferro-magnetic systems with a double polarization experiment, the major improvement is in increasing the magnitude of the observed effects, at the cost of raw signal rate. In non-magnetic systems with single polarization, no effect is observed. In order to see the underlying spin characteristics in non-magnetic systems, one must resort to double polarization experiments (Fig. 10).

The Pu spectrum shown in Fig. 9 is a simulated spin dichroism spectrum, based upon the theoretical model developed in Section 3 and illustrated in Figs. 6–8. As a test of this model, it has also been applied to the case of the Au 4f Fano effect, as shown in Fig. 11. Clearly, even with this simple model the essence of the spin dichroic behavior is captured, generating almost quantitative agreement with the experimental results.

The investigation is being pursued in a two-pronged fashion: (a) calibration studies of Ce, the 4f analogue of Pu, at synchrotron radiation sources; and (b) in house studies of Pu.

Although we have not yet been able to carry out the Pu double polarization experiment, we have been able to test the feasibility of this approach using Ce, the rare earth element analogue of Pu. Shown in Fig. 12 are the preliminary results for double polarization photoelectron spectroscopy of polycrystalline γ-Ce, using both a chiral excitation source (such as circularly polarized X-rays) and spin resolving detection [25–27].

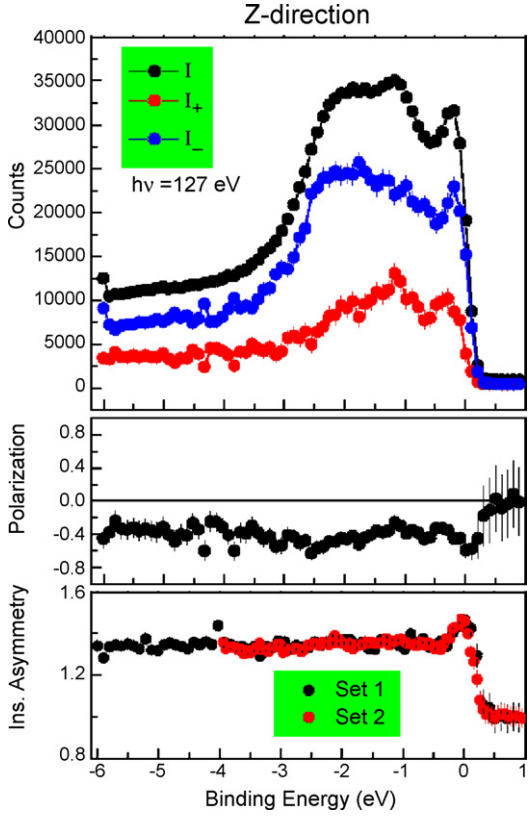

Fig. 12. Fano PES results from Ce, from [26].

5. Pu summary

The correct Hamiltonian for Pu is being converged upon.

Proven: Pu is a jj-skewed intermediate coupling case, NOT LS (Russell-Saunders).
Proven: V_{SO} » Vocalization
Strong Indications for δ-Pu: V_{MAG} perturbs V_{SO} and $V_{MAG} > V_{Delocalization}$
Possibly: There is an additional cancellation going on in δ-Pu, such as Kondo shielding, spin fluctuation, non-collinearity, or averaging.

We can resolve these last two issues with the Fano effect measurements. Probable ordering

$$\alpha - \text{Pu 5f} : V_{SO} > V_{MAG} \approx V_{Delocalization} > 0.$$
$$\delta - \text{Pu 5f} : V_{SO} > V_{MAG} > V_{Delocalization} > 0.$$

Acknowledgement

This work was performed under the auspices of the U.S. DOE by University of California Lawrence Livermore National Laboratory under contract W-7405-Eng-48. Work by LLNL personnel was funded in part by the Office of Basic Energy Science at DOE. The ALS and the Beamline 4 Spectromicroscopy Facility have been built and operated under funding from the Office of Basic Energy Science at DOE.

References

[1] J.G. Tobin, B.W. Chung, R.K. Schulze, J. Terry, J.D. Farr, D.K. Shuh, K. Heinzelman, E. Rotenberg, G.D. Waddill, G. Van der Laan, Phys. Rev. B 68 (2003) 155109.

[2] K.T. Moore, M.A. Wall, A.J. Schwartz, B.W. Chung, D.K. Shuh, R.K. Schulze, J.G. Tobin, Phys. Rev. Lett. 90 (2003) 196404.

[3] G. van der Laan, K.T. Moore, J.G. Tobin, B.W. Chung, M.A. Wall, A.J. Schwartz, Phys. Rev. Lett. 93 (2004) 097401;
K.T. Moore, G. van der Laan, R.G. Haire, M.A. Wall, A.J. Schwartz, Phys. Rev. B 73 (2006) 033109.

[4] J.G. Tobin, K.T. Moore, B.W. Chung, M.A. Wall, A.J. Schwartz, G. van der Laan, A.L. Kutepov, Phys. Rev. B 72 (2005) 085109.

[5] S.Y. Savrosov, G. Kotliar, Phys. Rev. Lett. 84 (2000) 3670.

[6] P. Soderlind, EuroPhys. Lett. 55 (2001) 525.

[7] P. Soderlind, A. Landa, B. Sadigh, Phys. Rev. B 66 (2002) 205109.

[8] B. Sadigh, P. Soderlind, W.G. Wolfer, Phys. Rev. B 68 (2003) 241101.

[9] P. Soderlind, B. Sadigh, Phys. Rev. Lett. 92 (2004) 185702.

[10] A.L. Kutepov, S.G. Kutepova, J. Phys. Cond. Matter 15 (2003) 2607;
A.L. Kutepov, private communication, UCRL-TR-200654.

[11] G. Kotliar, D. Vollhardt, Phys. Today 57 (2004) 53.

[12] R.C. Albers, Nature 410 (2001) 759.

[13] S.Y. Savrasov, G. Kotliar, E. Abrahams, Nature 410 (2001) 793.

[14] A.J. Arko, M.B. Brodsky, N.J. Nellis, Phys. Rev. B 5 (1972) 4564.

[15] Michael Brookes, ITU. Germany, private communication.

[16] J. Lashley, A. Lawson, R.B. McQueeney, G.H. Lander, Phys. Rev. B 72 (2005) 054416 [and references therein].

[17] W.J. Nellis, M.B. Brodsky, Magnetic Properties, in: A.J. Freeman, S. Darby (Eds.), The Actinides: Electronic Structure and Related Properties, vol. 2, Academic, New York, 1974.

[18] J.G. Tobin, F.O. Schumann, Surf. Sci. 478 (2001) 211.

[19] M.T. Butterfield, T. Durakiewicz, E. Guziewicz, J.J. Joyce, A.J. Arko, D.P. Moore, L. Morales, Surf. Sci. 571 (2004) 74.

[20] J.R. Naegele, L. Manes, J.C. Spirlet, W. Muller, Phys. Rev. Lett. 52 (1984) 1834–1837.

[21] U. Fano, Phys. Rev. 178 (1969) 131;
U. Fano, Phys. Rev. 184 (1969) 250.

[22] J. Kessler, J. Lorenz, Phys. Rev. Lett. 24 (1970) 87.

[23] G. Baum, M.S. Lubell, W. Raith, Phys. Rev. Lett. 25 (1970) 267.

[24] U. Heinzmann, J. Kessler, J. Lorenz, Phys. Rev. Lett. 25 (1970) 1325.

[25] S.W. Yu, T. Komesu, B.W. Chung, G.D. Waddill, S.A. Morton, J.G. Tobin, Phys. Rev. B 73 (2006) 075116.

[26] J.G. Tobin, S.A. Morton, B.W. Chung, S.W. Yuand, G.D. Waddill, Physica B 378–380 (2006) 925.

[27] J.G. Tobin, S.W. Yu, T. Komesu, B.W. Chung, S.A. Morton and G.D. Waddill, "Evidence of Dynamical Spin Shielding in Ce from Spin-Resolved Photoelectron Spectroscopy," Europhys. Lett. (2006), in press.